Acta Geodyn. Geomater., Vol. 20, No. 2 (210), 29–47, 2023
DOI: 10.13168/AGG.2023.0004
journal homepage: https://www.irsm.cas.cz/acta

ORIGINAL PAPER

ESTIMATION OF PRECIPITABLE WATER VAPOUR FROM GROUND BASED GPS MEASUREMENTS AND RADIOSONDE DATA IN SOUTHEAST ASIAN-PACIFIC

Jabir Shabbir MALIK [1), *] and Ali Raza BARKET [2, 3)]

[1)] *School of Aerospace Engineering, Beijing Institute of Technology, Beijing 100081, China*
[2)] *School of Information and Electronics, Beijing Institute of Technology, Beijing 100081, China*
[3)] *Department of Computer Science, Sukkur IBA University, Sukkur, Pakistan*

**Corresponding author's e-mail::* jsmalik@bit.edu.cn

ARTICLE INFO

Article history:
Received 19 February 2023
Accepted 6 June 2023
Available online 19 June 2023

Keywords:
Precipitable water vapor
GAMP
GPS
Radiosonde

ABSTRACT

Climate change research is an important field of study. Because of the refractivity of the earth's atmosphere, Global Positioning System (GPS) signals have a significant delay, making them a suitable approach for studying atmospheric weather phenomena. The zenith wet delays (ZWD) can be determined using GPS measurements. The capability of computing precipitable water vapour (PWV) from GPS signals is helpful to comprehend unique weather events. There are two objective for this work, firstly, zenith tropospheric delay (ZTD) is estimated for total of 20 GPS stations. Results demonstrated that the average root mean square (RMS) and standard deviation (STD) of ZTD estimate is 2440.1 and 63.6 mm, respectively. We compared the calculated ZTD values with the ZTD products offered by Center of Orbit Determination in Europe (CODE) products. Comparison results showed that the average difference and STD between estimates of ZTD and CODE products is 4.84 and 3.77 mm, respectively. Secondly, estimates of ZWD is used to determine the PWV. According to the PWV estimation results, the average RMS and STD value is 35.89 and 11.14 mm, respectively. PWV estimates for 10 IGS sites are compared with Radiosonde (RS) data. Comparison results show that the GPS-PWV estimates and RS data that the R's squared, bias and difference in STD is, respectively, 0.94, -0.24 and 3.99 mm. In addition, the differences of STD between RS-PWV and GPS-PWV is 3.88 and 4.08 mm, at UTC 00:00 and UTC 12:00, respectively.

1. INTRODUCTION

Earth's atmosphere can be divided into sub-regions since modelling it requires a great deal of complexity. Each zone of the atmosphere is distinguished from one another by ionization, temperature, and propagation (Jin et al., 2014; Jin, 2012). The tropospheric zone in the atmosphere ranges between 0-12 km in altitude and having a temperature that is linearly decreasing (Gleason and Gebre-Egziabher, 2009). Zenith wet delays (ZWD) is the main component of interest for geodesists and meteorologists. The average ZWD has a variability of 40 % (Jin et al., 2014). Filtering ZWD is quite useful in space geodesy, because this parameter can be converted into precipitable water vapour (PWV) or integrated water vapour (IWV).

Permanent and continuous observations with wide spatial distributions, outstanding accuracy, as well as data from all-weather working conditions are all possible with Global Positioning System (GPS) technology. More than twenty years of research and comparison with radiosonde (RS), Radio occultation (RO) and Very Long Baseline Inteferometry (VLBI), GPS ZWD have been shown to be a reliable water vapour sensor for meteorology, atmospheric and global weather applications (Wang and Zhang, 2009; Boccolari et al., 2003; Jin and Luo, 2009; Singh et al., 2014). GPS ZWD can be utilized for both large-scale analyses and numerical weather data assimilation or forecast models (Zhao et al., 2020).

The Southeast Asian-Pacific area has a significant effect on weather and climate. The area that is classified as maritime continent, tropics, islands and oceans. The typical geographical location and topography lead to the formation of the Tropical Warm Pool (TWP), which is the world's warmest large area of ocean (Kuleshov et al., 2014). Tropical cyclones, known as typhoons in the Pacific, also bring a lot of rain to Southeast Asia countries. Typhoons often originate in the Central Pacific and sweep westward over Southeast Asia. Southeast Asia has relatively high temperatures, relative humidity, and considerable precipitation. Another key climate driver is the El Nio-Southern Oscillation (ENSO), a combined ocean-atmosphere phenomena in the Southeast Asia and central Pacific as well (Trenberth, 1997). As a result, the seasonal monsoon pattern can trigger severe weather phenomena such as floods and droughts (Abram et al., 2020).

PWV can be obtained by using surface meteorological measurements. However, data from several numerical models are used in the absence of

Cite this article as: Malik JS, Barket AR: Estimation of precipitable water vapor from ground based GPS measurements and Radiosonde in Southeast Asian-Pacific. Acta Geodyn. Geomater., 19, No. 2 (210), 29–47, 2023. DOI: 10.13168/AGG.2023.0004

surface meteorological data. Accuracy of these models vary and depends on region, season, and other environment factors. To correct tropospheric delays or transform ZWD into PWV, Numerous Weather Models (NWM) have been developed and studied (Bennitt and Jupp, 2012). However, these models' performance is hindered by their low resolutions. The possibility to remove this restriction arises with the announcement of European Centre for Medium-Range Weather Forecasts Re-Analysis 5 (ERA5) data (Zhang et al., 2018; Sun et al., 2019; Hersbach et al., 2020). Many aspects of ERA5 have been updated and innovated, including an increase in the amount of data assimilated. In order to build a worldwide temperature (T), pressure (P), and ZTD model, ERA5 is therefore promising data resource.

In previous studies, geographical locations and seasons can have a significant impact on Mapping Function (MF), introducing various potential and systematic biases from station to station. (Ohtani and Naito, 2000), evaluated the accuracy and characteristics of Japan's (PWV) and verified GPS estimated PWV with those obtained from the 10 closest RS sites. Results revealed that the mean bias between GPS PWV and RS PWV at 12:00 UTC was consistently higher than at 00:00 UTC PWV results. In (Kwon et al., 2007), authors determined PWV from a GPS in the Korean Peninsula during two years of data and assessed results with RS measurements. With a STD of 2.45 mm, the mean bias between GPS PWV and RS PWV is 1.50 mm.

In other research (Musa et al., 2011), GPS data in Peninsular Malaysia were assessed for accuracy of IWV. Double difference (DD) GPS data processing was used to evaluate four GPS stations. The results demonstrated that the GPS-IWV have root mean square errors (RMSE) of 3.4 – 4.2 kg/m^2, respectively, and linear correlation coefficients of 0.79 – 0.88 for the four GPS stations. Choy et al. (2015), compared the atmospheric GPS PWV in Australia with RS measurements as well as the VLBI method over a 5-year period. Authors showed that the mean difference and STD between GPS and RS PWV measurements of 0.1 mm and 4.0 mm, respectively. It was also demonstrated how the amount of atmospheric moisture affects the size and range of PWV estimates.

In (Gui et al., 2017), authors studied and examined the spatial variation of PWV in China from two years of data. Authors compared GPS PWV, RS PWV, Moderate resolution Imaging Spectro-radiometer near-infrared (MODIS-NIR) Clear-PWV and Aerosol Robotic Network sunphotometer (AERONET) PWV were the four PWV products. The findings of the study showed that the correlation between GPS-PWV and RS-PWV was slightly stronger at 00:00 UTC than at 12:00 UTC. At 00:00 UTC and 12:00 UTC, respectively, the mean values of the bias and STD between GPS PWV and RS PWV was 0.23 and 2.76 mm, respectively.

Another work to estimate PWV carried out by (Ssenyunzi et al., 2020) uses GPS data from 13 stations. The GPS PWV computed from MET data and the GPS PWV derived using the ERA5 interpolated data. The maximum PWV values are found in spring and summer at the stations between latitudes 4S and 4N and latitudes 12S and 4S, respectively, whereas the lowest values are found in summer and winter seasons at these locations.

Numerous studies have demonstrated that "GPS meteorology" may be used in conjunction with other remote-sensing methods to estimate water vapour concentration since it provides thorough coverage. Furthermore, quality, consistency, and accuracy of GPS satellite orbit and clock products is relatively high than the accuracy performance of the GLONASS, BeiDou and Galileo navigation systems. Therefore, GPS observations can be used for determining the PWV.

The aim of this work is to analyse ZTD estimates obtained with GPS observations from twenty stations. Compare the ZTD estimates from the ZTD true product of the same day epoch by epoch in order to assess the quality of the ZTD estimates. The second aim of the work is to process the ZWD and conversion to GPS PWV estimates in order to examine variations in PW estimates. Then, PWV estimate results are gathered by four different months in order to evaluate the PWV variations. The current work is comprised of three parts: (a) ZTD estimation from GPS data, (b) transformation of ZWD to PWV, (c) comparison of the PWV determined by GPS with the RS PWV data. The primary objective of this work is to investigate variation of PWV in Southeast Asian-Pacific area.

2. ESTIMATION METHODOLOGY

In this study, Precise Point Positioning (PPP) mode is adopted to estimate zenith tropospheric delay (ZTD) (Zumberge et al., 1997). There are two types of tropospheric delay: a zenith wet delay (ZWD) principally brought on by water vapour and a zenith hydrostatic delay (ZHD) caused by atmospheric gases (Jin et al., 2014). Typically, each component is viewed as the sum of the zenith delay and the corresponding mapping functions, as follows;

$$T^r = (ZWD.w_w(s) + ZHD.w_h(s) + w_g(s)) \qquad (1)$$

In Equation (1), s is elevation of the satellite; w_w, w_h, and w_g shows wet, hydrostatic, and gradient component, respectively; w_h and w_w are retrieved with Mapping Functions (MF). In this study, Global Mapping Function (GMF) in-combination with the Global Pressure and Temperature2 (GPT2) version is employed. The GPT2 is an empirical model, which uses data from 2001 to 2010. In order to perfectly account for areas with predominant rainy or very dry seasons, European Centre for Medium-Range Weather Forecasts (ECMWF) monthly mean profiles data is utilized (Boehm et al., 2006b; Boehm et al., 2006a). Additionally, GMF (GPT2) is better able to replicate the tropospheric delay, which is affected by

atmospheric variables (such as temperature, pressure, and partial water pressure) close to the GPS receiver. Furthermore, ZWD and gradient function w_g is estimated as unknown parameters in the PPP processing. In order to model ZHD, Saastamoinen model is used (Saastamoinen, 1972).

$$ZHD = \frac{0.0022768P^{GNSS}}{1-0.00266cos2\varphi-0.0028H} \quad (2)$$

Where P^{GNSS} shows the surface pressure (hPa), φ shows GPS site latitude in radians, and *H* is the height from mean sea level in meter. To determine the precipitable water vapour (PWV), ZWD is transformed into PWV by utilizing the conversion factor Q

$$PWV = Q.ZWD \quad (3)$$

Herein, conversion factor Q (dimensionless quantity) can be calculated using surface measurements (Alshawaf et al., 2015);

$$Q = \frac{10^6}{\rho_v R_v(\frac{k_3}{T_m}+k_2')} \quad (4)$$

Where ρ_v (1000 Kg/m-3) and R_v (461.465 $JKg^{-1}K^{-1}$) is the density and specific gas constant of water vapour, respectively. While, k_3 (22±0.000021 kpa^{-1}) and k_2' (3.75±0.033487 K^2 Kpa^{-1}) represents the refraction constants. T_m is the weighted mean temperature in Kelvin, which is written as.

$$T_m = \frac{\int_{p1}^{p2}\frac{P_v}{T}dp}{\int_{p1}^{p2}\frac{P_v}{T}dp} \quad (5)$$

Where p^1 and p^2 shows the air partial pressure at level P_1 and P_2, T is the temperature for the corresponding pressure level. T_m can be calculated and estimated using empirical linear relationship model as mentioned in (Bevis et al. 1992) and studied and investigated by several authors (Jin and Luo, 2009; Singh et al., 2014; Cao et al., 2016), and written as;

$$T_m = 0.72T_s + 70.2 \quad (6)$$

In Equation (6), T_s shows surface temperature in kelvin. Meanwhile, some scientists found that the above regression line is somehow weak, particularly in the tropics. This suggests that the Bevis model cannot accurately reflect the actual global climate. There have been initiatives to enhance global T_m models like the one presented by (Yao et al., 2014;Yao et al., 2012). They conducted research to modify the Bevis model, using 135 globally dispersed radiosonde sites during a ten-year period, and came to the following conclusions.

$$T_m = 0.8116T_s + 43.69 \quad (7)$$

Finding at least one meteorological site nearby is necessary when the GPS station does not have meteorological sensor accessible. The meteorological observatory can be 100 km away since temperature variation is greater in the vertical than in the horizontal direction. As a result, when using meteorological data from a nearby meteorological station, pressure and temperature at the GPS site is computed by taking the altitude difference into account. The temperature is computed at the GPS station T_{GPS}, because it varies linearly with station height.

$$T_{GPS} = T_{MET} - L(h_{GPS} - h_{MET}) \quad (8)$$

In Equation (8), T_{MET} denotes the measured temperature at meteorological station and L defines the temperature lapse rate (0.0065 $^oCm^{-1}$); h_{GPS} and h_{MET} shows the corresponding height of GPS and meteorological site, respectively.

In this work, we employed GAMP (GNSS Analysis software for Multi-constellation and multi-frequency precise) positioning (Zhou et al., 2018; Malik et al., 2020). The spectral density for ZTD is set to 1.0×10^{-8} m^2/sec. The precise orbit and clock products provided by multi GNSS experiment (MGEX) analysis center-GFZ (GeoForschungsZentrum Potsdam) (Prange et al., 2020) applied for correction. Table 1 lists the parameters used to process the GPS data and ZTD estimation.

2.1. STUDY AREA

A total of 20 GPS stations are utilized for the year 2019. Figure 1 shows the geographical locations of the stations including GPS, radiosonde (RS) and meteorological sites used for this study. Table 2 shows the information about GPS stations coordinates.

The PWV values derived from GPS observations are examined and compared with the 10 RS sites. It can be seen from the Table 2 that LHAZ station has very high ellipsoidal height (~ 3622.0 m) and followed by 665.37 m height for TIDB station (35°S). However, minimum heigh t of study area is at COCO site, which is –35.2 m. Table 3 displays the separations in height and distance between GPS and nearby RS stations. RS data is available at: https://www.ncei.noaa.gov/data/integrated-global-radiosonde-archive/. In addition, chosen RS stations are relatively near the GPS site and the shortest distance between the GPS and RS sites is about 75 kilometres. Not all of the GPS stations have the meteorological sensors installed, so data for the surface temperature (T) and surface pressure (P) are acquired from meteorological sites that are close to where the GPS sites are located. The weather data can be accessed at, https://www.ncei.noaa.gov/data/global-summary-of-the-day/access/. On a daily basis, the pressure (mbar), mean surface temperature (°C) of the surface meteorological data have 1-hour temporal resolution. Table 4 shows the location of the closest weather meteorological sites. In this study, 13 meteorological stations are used to estimate the PWV. We applied equation (8) to interpolate the surface temperature and height of the meteorological station into GPS coordinates.

Table 1 Summary and an overview of approach for precipitable water vapour estimates.

Constellation	*GPS system*
Satellite orbit and clock	Precise products from (MGEX -GFZ) center
Satellite and Receiver antenna phase center (PCOs/PCVs)	IGS antenna model IGS14.atx
Troposphere	
Dry part	Apriori values (Saastamoinen model)
Wet part	Global Mapping Function (GMF)
Filter	Kalman Filter
Satellite mask	5^0
Weighting scheme	Elevation dependent
Priori observation	Carrier phase (0.03 cm): Code pseudoranges (3.0 cm)
Solid earth tides, Phase wind up, Ocean tide loading, and Relativistic effect	International Earth Rotation and Reference System (IERS 2010) Corrections applied

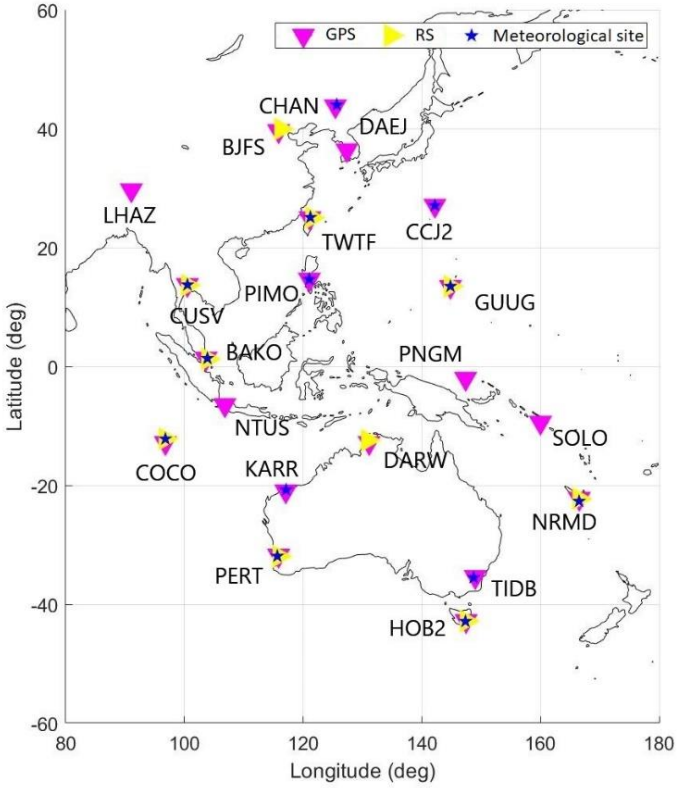

Fig. 1 Location of the GPS, Radiosonde (RS) and weather meteorological sites.

3. RESULTS

3.1. ANALYSIS OF ZTD

In this section, estimates of zenith tropospheric delay (ZTD) is discussed and analysed. In order to compare ZTD estimates, Center for Orbit Determination in Europe (CODE) daily products are utilized. Additionally, CODE ZTD products are sampled with every 5 (minute) resolution epoch (Kouba, 2009; Hakman et al., 2015)

Standard deviation (STD) and Root mean square (RMS) is computed for each of the GPS stations. The RMS and STD are used as performance indicators to analyse the ZTD estimates. STD is a metric that reveals how much variation from the PPP mean solution exists. Figure 2 shows the average STD of the ZTD estimates for selected area of the study during month of January/February (JF), April/May (AM), July/August (JA) and October/November (ON). While, results obtained for chosen stations during JF, AM, JA and ON months are shown in Table 5. Table 6 outlines the annual estimates of ZTD for the selected 20 stations.

Table 2 GPS station coordinates and height information.

GPS site	Lat. (°)	Long. (°)	Height (m)
BAKO	-6.49	106.85	158.2
BJFS	39.6	115.89	87.4
CCJ2	27.06	142.19	104.2
CHAN	43.79	125.44	268.3
CUSV	13.73	100.53	76.1
COCO	-12.18	96.83	-35.2
DAEJ	36.39	127.37	117
DARW	-12.84	131.13	125.2
GUUG	13.43	144.8	134.7
HOB2	-42.8	147.43	41.1
KARR	-20.98	117.09	109.2
LHAZ	29.65	91.1	3622
NTUS	1.34	103.67	79
PERT	-31.8	115.88	12.9
PIMO	14.63	121.07	95.5
TIDB	-35.39	148.97	665.4
TWTF	24.95	121.16	203.1
PNMG	-2.04	147.36	116.3
SOLO	-9.43	159.95	122.9
NRMD	-22.22	166.48	160.4

Table 4 Surface meteorological stations used for the studv.

ID	Long. (°)	Lat. (°)	Elevation (m)
479710	142.191	27.092	8
541610	125.681	43.996	215.18
912120	144.8	13.483	77.4
484550	100.567	13.733	4
949700	147.333	-42.883	51
943080	117.15	-20.75	11
946080	115.867	-31.916	25
915920	166.45	-22.267	72
466860	121.233	25.078	32
486940	103.91	1.36	19
984300	121.05	14.65	46
969960	96.834	-12.188	3
959250	148.767	-35.533	1760

Table 3 Distance and height differences between GPS and radiosonde sites

GPS	RS site	ΔH (m)	Distance between IGS and RS (km)
BJFS	CHM54511	55.10	49
GUUG	GQM91212	59.30	5
CUSV	THM48453	11.00	75.3
COCO	CKM96996	-37.20	0
DARW	ASM94120	94.80	53
TWTF	TWM58968	194.10	37
NTUS	SNM48698	74.00	34
NRMD	NCM91592	90.38	6
HOB2	ASM94975	37.10	6
PERT	ASM94610	7.50	16

Table 5 Root mean square (RMS) of ZTD estimates for January/February, April/May, July/August and October/November time period (unit: mm).

Site	JF	AM	JA	ON
BAKO	2601.6	2602.3	2551.3	2552.3
BJFS	2342.4	2363.5	2503.6	2383.1
CCJ2	2430.7	2491.7	2610	2545.8
CHAN	2284.6	2314.4	2414.2	2302.3
CUSV	2448.7	2580.6	2638.8	2583.3
COCO	2637.5	2637.5	2564.4	2561.7
DAEJ	2349.2	2388.8	2549	2395.2
DARW	2605.8	2532.7	2430.5	2523.9
GUUG	2503.5	2531.5	2620.7	2591.3
HOB2	2416.9	2398.6	2371.5	2380.7
KARR	2495.8	2440.8	2418.3	2408.5
LHAZ	1499.3	1546.6	1629.2	1530.6
NTUS	2590.3	2616.1	2572	2611.3
NRMD	2529	2489.2	2443.7	2482
PERT	2418.7	2412.1	2410.4	2402.8
PIMO	2485.2	2585.4	2645.3	2600.9
TIDB	2264.1	2252.2	2213.3	2241.7
TWTF	2404.9	2546	2573.5	2467.6
PNMG	2675.6	2661.2	2544.1	2598
SOLO	2630.5	2629.5	2583	2577.3
Mn	2430.7	2451	2464.3	2437

Analysis of Figure 2 and results given in Table 5 show that ZTD estimates are primarily depends on the specific area and location. On the other hand, it can be seen from results given in Table 5 that during JF, AM, JA and ON periods, the ZTD estimates has quiet comparable results for the stations at the equator. In addition, it can be shown from the results given in Table 5 that LHAZ station has very low ZTD estimates during JF, AM, JA and ON months, and ZTD estimate reaches to 1.40 – 1.60 m. While, estimates of ZTD reaches between 2.30 to 2.40 m for PERT, HOB2, KARR sites during JF, AM, JA and ON time periods at the stations between latitudes 20^0 S – 40^0 S. Furthermore, it can be demonstrated from the results given in Table 5 that the average RMS estimates of ZTD estimation for Southeast Asia-Pacific is 2.43 – 2.46 m during JF, AM, JA and ON time period. Additionally, average ZTD estimates for BAKO, COCO, GUUG, PNGM, SOLO and NTUS site is in range between 2.50 – 2.60 m.

Results given in Table 6 illustrate that the average RMS and STD value of ZTD estimate is 2440.1 and 63.6 mm, respectively. Figure 3 shows the ZTD difference between ZTD estimates and CODE products during JF, AM, JA and ON study period. Table 7 outlines the ZTD comparison results between estimates of ZTD and CODE products. Analysis of Figure 3 illustrates that the mean difference between the ZTD estimates and CODE products for the station BAKO is 10.0 and 9.0 mm during JF and AM month,

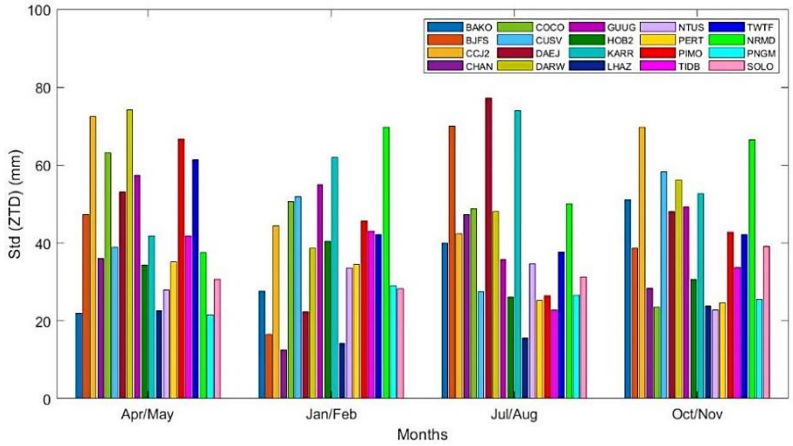

Fig. 2 Standard deviations of ZTD estimates for the different four months periods.

Table 6 Average root mean square (RMS) and standard deviation (STD) of ZTD estimates (unit: mm).

Site	RMS	STD	Site	RMS	STD
BAKO	2576.8	50.12	KARR	2445.1	75.68
BJFS	2398.7	74.36	LHAZ	1553.1	50.04
CCJ2	2521.3	89.57	NTUS	2596.7	41.31
CHAN	2329.4	59.31	PERT	2415.6	38.27
CUSV	2573.4	84.27	PIMO	2580.6	75.9
DAEJ	2422.2	90.83	TIDB	2245.7	42.77
DARW	2517.8	84.89	TWTF	2502.8	80.82
GUUG	2552.6	70.48	PNMG	2513.7	39.9
HOB2	2393.4	37.45	SOLO	2580.1	47.13
COCO	2600.2	73.18	NRMD	2483.3	65.72

Table 7 Mean difference and standard deviation (STD) difference between ZTD estimates and CODE products (unit: mm).

Site	Diff_mean	STD difference	Site	Diff_mean	STD difference
BAKO	8.37	5.12	KARR	5.14	3.69
BJFS	6.17	2.81	LHAZ	3.57	5.27
CCJ2	6.54	4.1	NTUS	6	3.17
CHAN	3.86	4.21	PERT	4.05	3.58
CUSV	5.22	4	PIMO	4.24	3.95
DAEJ	5.83	2.54	PNMG	5.21	4.62
DARW	4.62	3.4	SOLO	4.75	4.96
GUUG	4	4.09	TIDB	3.89	3.47
HOB2	3.67	3.22	TWTF	3.73	3.29
COCO	4.34	3.1	NRMD	3.65	2.94

respectively. Furthermore, difference between CODE products and ZTD estimates for BJFS, CCJ2, SOLO and NTUS stations is 8.0 mm during AM period. In addition, it can be demonstrated from Figure 3 that the mean difference between ZTD estimates and CODE products for KARR and TIDB site is about 6.0 – 6.5 mm during JA months. Results given in Table 7 demonstrates that average difference of STD between ZTD estimates and CODE products for BJFS, DAEJ and NRMD site is nearly 2.5 – 3.0 mm. While, difference of STD between IGS products and ZTD estimates is 5.0 mm for both BAKO and LHAZ stations, respectively. Furthermore, average difference and STD between estimates of ZTD and CODE products is 4.84 and 3.77 mm, respectively.

3.2. COMPARISON OF T_M CALCULATION

In this segment, regression line of Bevis model (Bevis et al., 1992) and Yao model (Yao et al., 2014) is studied for weighted mean temperature (T_m). Herein, Equation (6) and Equation (7) are applied to compute T_m for Bevis and Yao model, respectively. The time series for the T_m computations are displayed in Figure 4 and Figure 5 for DAEJ and PNGM station, respectively. It can be seen that both of the (Bevis model) and (Yao model) T_m formulas are in good agreement for DAEJ and PNGM as shown in Figure 4 and Figure 5, respectively. Table 8 summarizes the difference between two T_m formulas. Results shown in Table 8 illustrate that the mean values from both the (T_m - T_s) regression formulas are comparatively

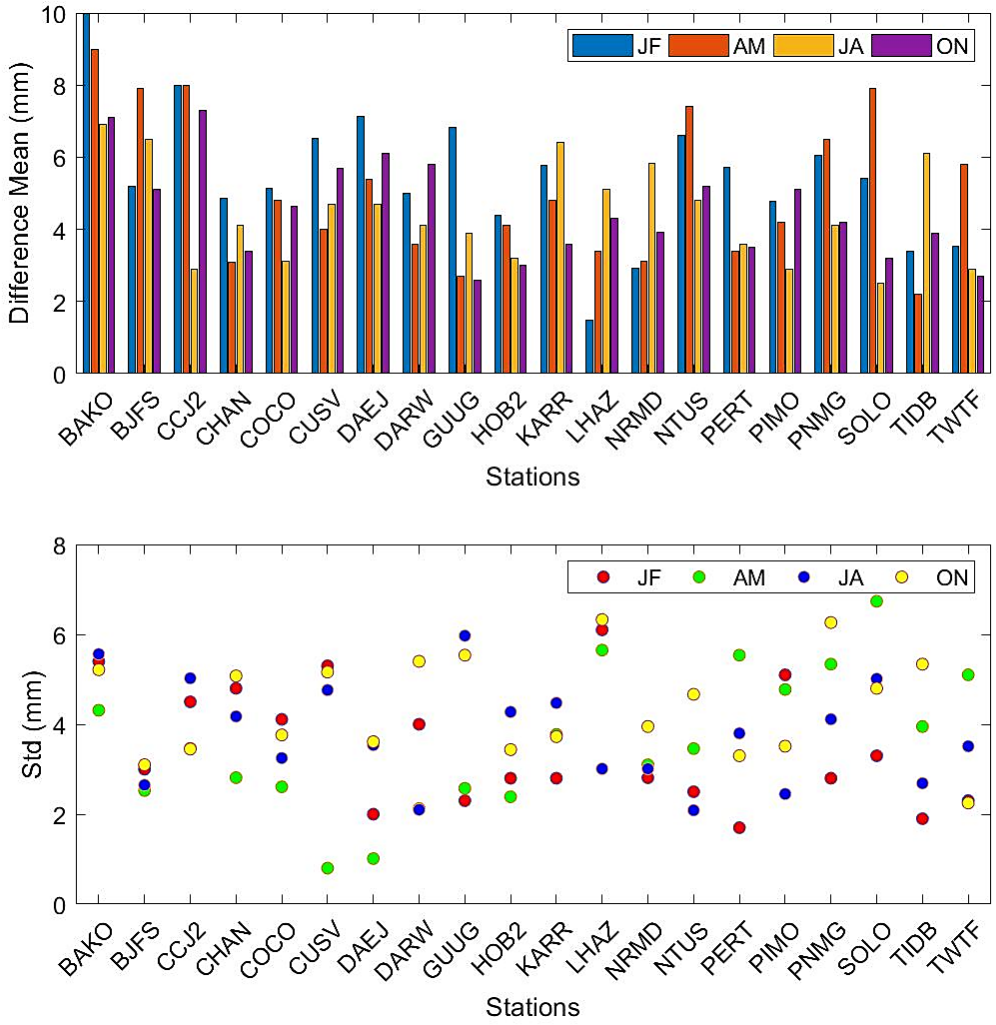

Fig. 3 Comparison between PPP ZTD estimates and CODE products for the selected 20 stations during JF, AM, JA, ON months. (above plot) ZTD average difference (below plot) Standard deviation difference.

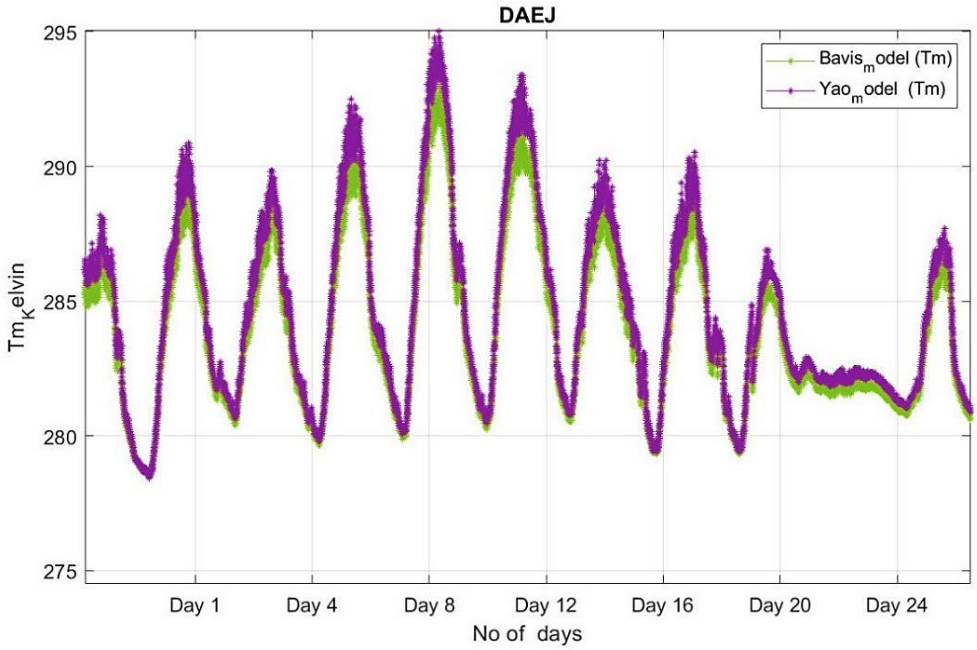

Fig. 4 Plot of Bevis (T_m-T_s) and Yao (T_m-T_s) model for DAEJ site.

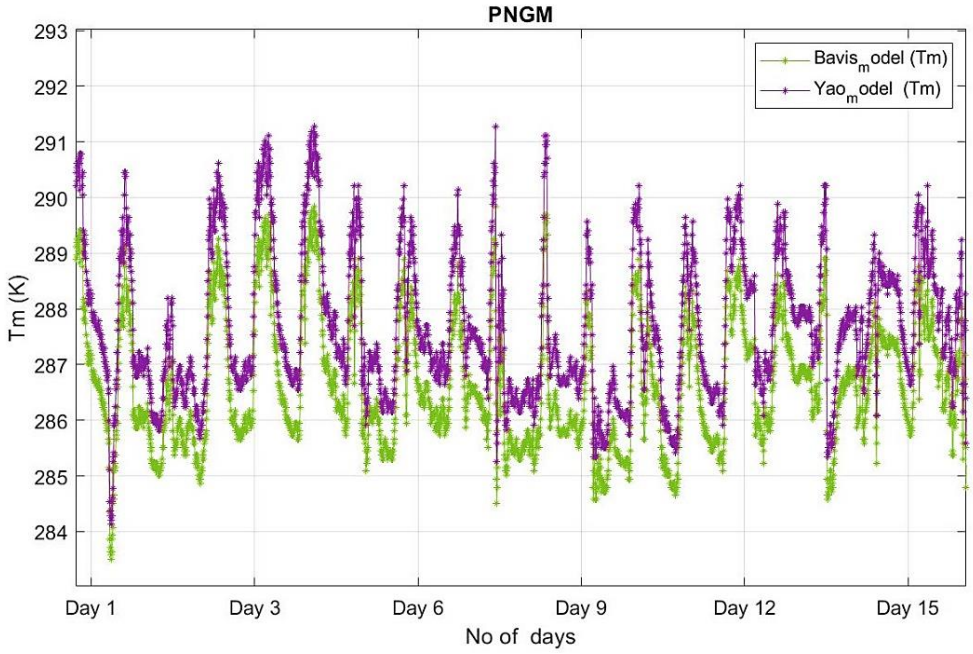

Fig. 5 Plot of Bavis (T_m-T_s) and Yao (T_m-T_s) models for PNGM site.

Table 8 Difference of Tm regression line between Yao (T_m) and Bavis (T_m) formulla.

Site	PWV difference (mm)	Mean difference (T_m in Kelvin)	STD difference (T_m in Kelvin)
DAEJ	0.01	-0.25	0.41
PNGM	0.21	1.02	0.14
CHAN	-0.02	-0.91	0.32
GUUG	0.14	1.01	0.16
LHAZ	-0.01	-0.63	0.37
Mn	0.07	0.23	0.27

similar. First, it can be observed that the daily cycle of the T_m computed by the regression formulas from both the Bevis and Yao model is more apparent. Another significant observation is that the mean difference and standard deviation (STD) difference between the Bevis model and Yao model for all stations is just 0.23 K and 0.27, respectively. Additionally, for each station, the mean bias between the Bevis model and Yao model ranges for the equatorial stations between 1.0 and 1.1 K. The region's very changing terrain and environment may be the cause of the Yao Tm's unique behavior in comparison to the Bevis model. Differences of the PWV estimates between the two models are also examined (Table 8). Results show that the average mean bias is nearly 0.07 mm (and STD of ~ 0.03 mm).

In Musa et al. (2017) authors revealed that PWV measurements from both the regression line (T_m - T_s) exhibit a high degree of agreement. T_m and T_s are warm throughout the year, with just a 1.0 – 2.0 K fluctuation. The T_m-T_s relationship was enhanced by segregating daytime and night time observations.

3.3. GPS PWV ESTIMATION

This section displays the GPS determined precipitable water vapour (PWV) for 20 stations. Variation of GPS PWV for the month of January/February (JF), April/May (AM), July/August (JA), and October/November (ON) are analyzed and discussed. Furthermore, annual average GPS PWV estimates for each site are also calculated and examined.

Figure 6 shows the bubble chart for GPS PWV estimates during JF, AM, JA and ON months. Table 9 displays the Root mean square (RMS) and standard deviation (STD) of GPS PWV estimates for 20 sites during January/February (JF), April/May (AM), July/August (JA), and October/November (ON) month. Table 10 provides average statistical results, maximum (Max), minimum (Min), standard deviation (STD) and root mean square (RMS) results annually.

Analysis of Figure 6 and results presented in the Table 10 indicate that PWV vary spatially from one geographic place to another concurrently. It can be demonstrated from Figure 6 that for all stations, GPS PWV estimates behavior for the month of JF, AM, JA, and ON varies considerably. GPS derived PWV values

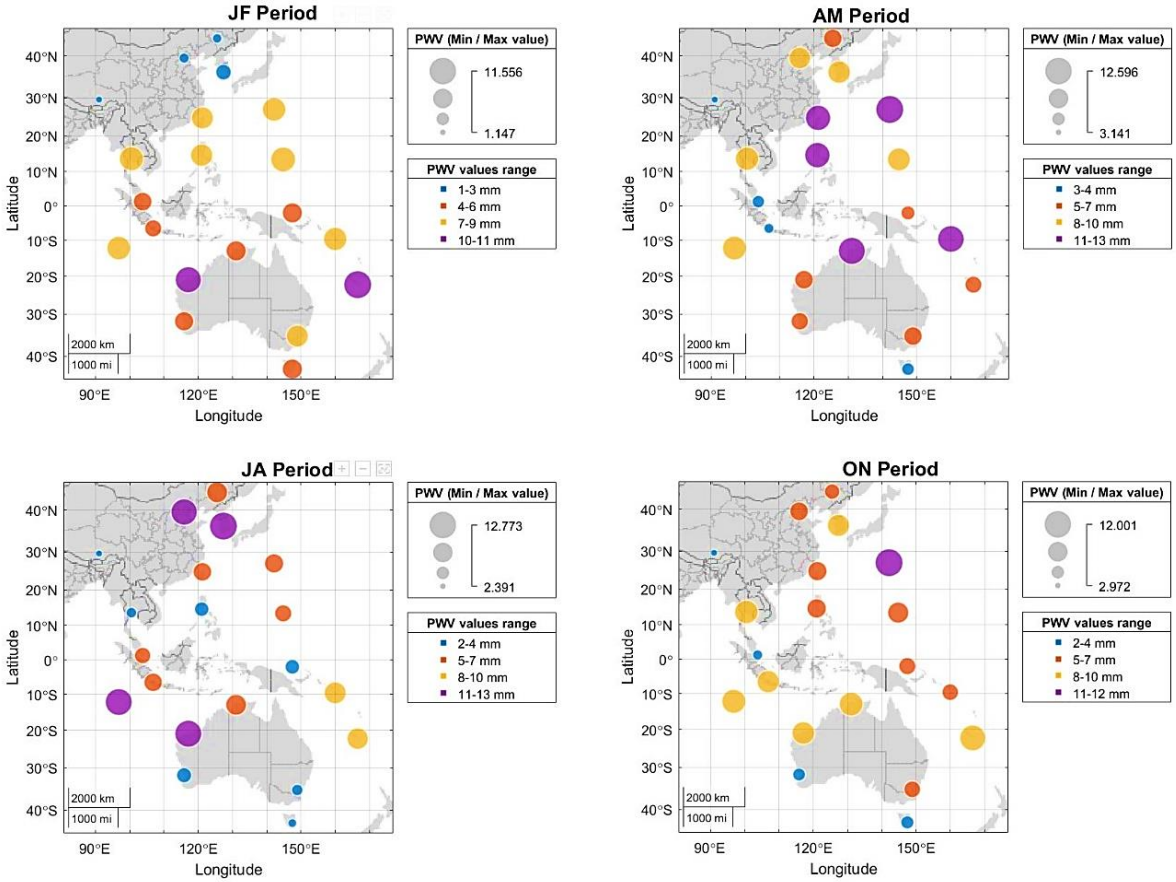

Fig. 6 Bubble chart of standard deviation for GPS PWV estimates during January/February, April/May, July/August, and October/November period.

Table 9 Statistical summary of GPS PWV estimates during four different months study period (unit: mm).

Site	JF		AM		JA		ON	
	RMS	STD	RMS	STD	RMS	STD	RMS	STD
BAKO	59.2	4.6	60.1	3.8	51.7	6.6	52.2	8.5
BJFS	4.2	1.9	16.2	8.6	40	11.6	13.4	6.7
CCJ2	20.7	8.2	32.2	12.6	51.2	6.9	40.6	12
CHAN	2.6	1.7	13.7	6.9	30.8	7.9	8.6	5.3
CUSV	29.5	8.7	51.7	10.5	59.8	3.3	50.2	9.2
COCO	55.3	8.4	55.6	9.9	43.3	11.9	42.7	9.5
DAEJ	6.9	3.9	18.6	9	46.7	12.8	16.7	8.4
DARW	53.1	6.2	41.2	11.9	23.2	7.8	39.9	9.3
GUUG	35.8	9.2	40.9	9.2	54.7	5.8	50.6	7.8
HOB2	20.7	6.2	15.8	4.6	12.4	2.8	15.2	4.5
KARR	38.3	10.2	27.3	6.9	24.5	12	23.8	8.7
LHAZ	2.7	1.1	9.6	3.1	21.7	2.4	6.3	2.9
NTUS	48.6	5.4	53.4	4.5	46.4	5.5	52.3	3.6
PERT	20.4	5.7	16.6	6.4	15.3	4.9	15.9	4.4
PIMO	30.9	7.5	48.9	10.8	58.1	4.6	50.7	7
TIDB	19.8	7.3	16.2	6.9	8.4	3.5	15.3	5.8
TWTF	21.7	7.3	48.3	10.8	53.8	6.6	32.7	6.9
PNMG	55	6.2	57.7	5	54.7	4.7	53.2	5.9
SOLO	53.9	8.1	53.9	11.7	46.2	8.5	53.7	5.7
NRMD	41.8	11.6	33.5	6.2	25.4	8.1	33.2	10.6
Mn	31.1	6.5	35.6	7.9	38.4	6.9	33.4	7.1

Table 10 Annual statistical results of GPS PWV for the stations used in the study (unit: mm).

Site	Max	Min	RMS	STD
BAKO	77.5	24.0	56.1	8.2
BJFS	71.3	0.2	22.2	14.6
CCJ2	67.4	6.8	38.3	15.9
CHAN	63.4	0.0	17.3	11.8
CUSV	75.1	8.2	50.5	13.9
COCO	74.2	18.9	49.6	12.1
DAEJ	72.8	0.9	26.5	16.7
DARW	71	2.9	39.9	12.5
GUUG	72	15.7	44.7	11.6
HOB2	44.5	2.4	16.3	5.6
KARR	71.9	3.2	30.5	12.9
LHAZ	27.1	0.3	12.3	7.5
NTUS	71.2	21.0	50.2	6.7
PERT	49.5	3.2	18.5	7.0
PIMO	77.9	14.4	48.4	12.8
TIDB	42.9	1.5	16.0	7.4
TWTF	74.9	3.3	41.5	15.3
PNMG	72.4	22.5	51.6	8.2
SOLO	75.8	17.8	54.1	10.9
NRMD	69.7	9.1	33.3	11.1

show significant difference between the results obtained during four different months study period. In addition, it can be clearly seen from the results given in Table 9 and Figure 6 that GPS PWV estimates during JA period sees a rapid increase, which then GPS PWV declines during ON period at sites between latitude 25º N – 35ºN. On the other hand, results given in Table 9 illustrate that GPS derived PWV STD values for the southern low latitude (TIDB, PERT, HOB2), GPS PWV continued to be quite low level during JA period, while GPS PWV estimate slightly increases during JF and ON period. Moreover, GPS PWV estimates for COCO station (latitude ~12˚S), RMS PWV results reach to 55.0 mm during JF and AM months, and PWV decreases to 42 – 43 mm during JA and ON months. Furthermore, it can be illustrated from results given in Table 9 that the RMS of PWV estimates for CCJ2 station is relatively high in JA month and reaches to 51.16 mm, while during ON month RMS is 40.59 mm. In addition, the GPS PWV results for BJFS and CHAN station is the lowest during JF and AM months, while PWV estimates increases during JA period and PWV values is start decreasing during ON period. Additionally, for stations between latitudes 15˚N – 10˚S (i.e., NTUS, PNGM, SOLO, BAKO, CUSV, GUUG, PIMO), GPS PWV values are higher during the study period. Furthermore, GPS PWV estimate for tropical stations (BAKO, CUSV, GUUG, PIMO, NTUS), is high during the period of JA and ON, relatively high PWV estimate at these stations may be due to the East Asian summer monsoon.

Likewise, PWV estimate is also high for stations in mid-latitude stations (CCJ2, DAEJ, BJFS, DAEJ), in JA period. Moreover, PWV content at NRMD station (22˚S/166°E) is generally high and RMS of PWV estimate is 41.77 and 25.0 mm during JF and JA month, respectively. This may be due to the local climate, which is substantially more humid and whole local weather is controlled by the South Pacific Convergence zone (SPCZ).

(Haffke and Magnusdottir, 2013). Moreover, outcome show that the average STD of GPS PWV estimate is 6.5, 7.9, 6.9 and 7.1 mm during JF, AM, JA and ON month study period, respectively. The annual STD for GPS PWV estimate for the 20 stations is displayed in Figure 7. Average STD of GPS PWV estimate is 11.1 mm. Table 11 summarizes GPS PWV estimate statistical results based on geographical stations location (Latitude). Results given in Table 11 demonstrate that, as compare to the PWV estimate at latitude side, the PWV variability along the longitude is less notable. Additionally, there is a considerable variation in PWV estimate at the study stations. Results given in Table 11 show that, RMS of GPS PWV is 16 to 17 mm with the relatively dry atmosphere in latitude between (41˚N – 45°N and 35°S – 45°S) and RMS is 30 mm to 47 mm with the wet atmosphere at the stations latitude between (11°N – 15°N and 11°S – 25°S). Moreover, tropical stations in the latitude between 5°N and 10°S that are moderately humid and wet, RMS of PWV estimate is 50 to 55 mm.

3.4. PWV COMPARISON WITH RS

In this section, GPS derived precipitable water vapour (GPS-PWV) and Radiosonde measured PWV (RS-PWV) for 10 stations is discussed in detail. Comparison and assessments of GPS-PWV and RS-PWV is examined at 00:00 UTC and 12:00 UTC. Radiosonde has been reported in the literature as having its own systematic bias of approximately 1.2 – 1.5 mm based on the types of radiosonde. RS-PWV observations have traditionally and frequently been utilized against other instrument/sensors for PWV measurements. The GPS-PWV statistical comparison is conducted for the same RS-PWV matched epoch. We used the statistical tools i.e., Bias and the correlation coefficient between the GPS - derived

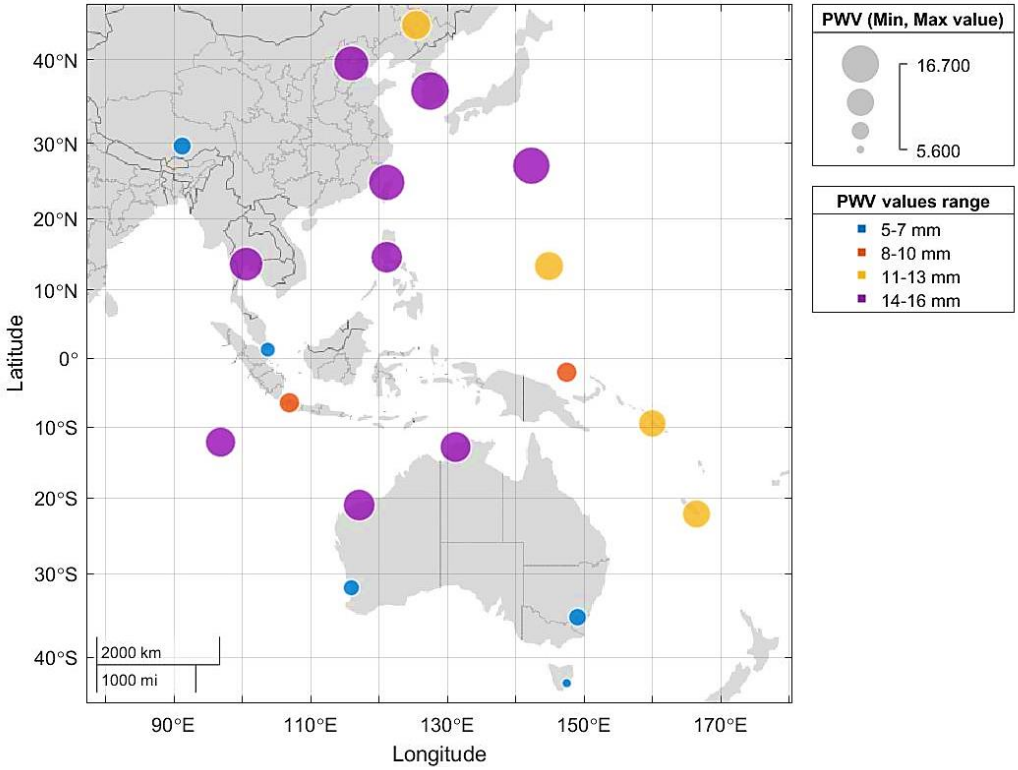

Fig. 7 Bubble chart of standard deviation for GPS PWV estimates.

Table 11 Annual statistical results of GPS PWV for the stations used in the study (unit: mm).

Site	Max	Min	RMS	STD
0-5N	71.2	21	50.2	6.7
11-15N	75	12.7	47.8	12.7
21-25N	74.9	3.3	41.5	15.3
26-30N	47.3	3.55	25.3	11.7
36-40N	72.1	0.55	24.4	15.6
41-45N	63.4	0	17.3	11.8
0-5S	72.4	22.5	51.6	8.2
6-10S	76.6	20.9	55.1	9.55
11-15S	72.6	10.9	44.7	12.3
16-20S	71.9	3.2	30.5	12.9
21-25S	69.7	9.1	33.3	11.1
31-35S	46.2	2.4	17.3	7.2
41-45S	44.5	2.4	16.3	5.6

PWV and measured value of RS-PWV time series, as follows:

$$Bias = \frac{1}{n}\sum_{i=1}^{n}(k_i - l_i) \quad (9)$$

In Equation (9), k_i and l_i is the time series of the estimated GPS-PWV and measured RS-PWV values. In addition, correlation between the GPS-PWV and measured RS-PWV values is determined by squaring the Pearson correlation (R^2), written as;

$$R = \frac{n\sum pq - (\sum p)(\sum q)}{\sqrt{n(\sum p^2) - (\sum p)^2} - \sqrt{n(\sum q^2) - (\sum q)^2}} \quad (10)$$

In Equation (10), n shows data points, p and q represents the RS-PWV and GPS-PWV values, respectively. A strong correlation between the two-time series i.e., RS-PWV and GPS-derived PWV is shown by a high value of R^2. Figure 8 displays the scatter plot between GPS-PWV and RS-PWV for BJFS, DARW, GUUG, HOB2, NRMD, NTUS, PERT and TWTF sites.

Figure 9 and Figure 10 display the comparison of GPS-PWV estimates against the RS-PWV measurements for stations BJFS, DARW, GUUG, HOB2 and NRMD, NTUS, PERT, TWTF stations, respectively. While Figure 11 presents the scatter plot and annual observations of GPS-PWV against RS-PWV estimates at CUSV and COCO site at 00:00 UTC only. This is because RS-PWV measurements only available at UTC 00:00.

Table 12 and Table 13 present the statistical results of GPS-derived PWV estimate against RS-measured PWV at 0000 UTC and 1200 UTC, respectively. Analysis of Figure 8 – Figure 11 demonstrates that the PWV obtained from GPS and

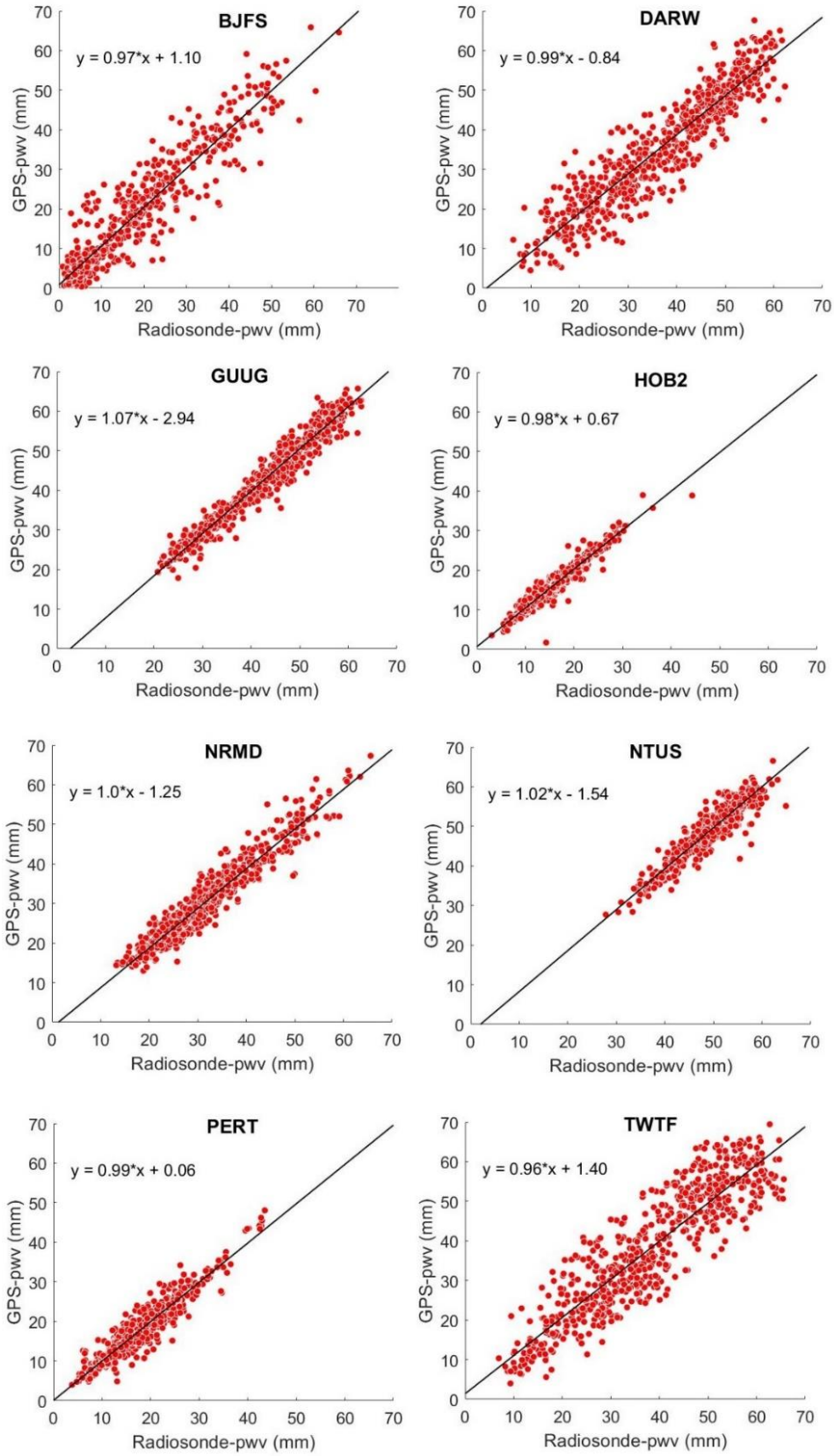

Fig. 8 Scatter plot of GPS PWV against RS PWV measurements for BJFS, DARW, GUUG, HOB2, NRMD, NTUS, PERT and TWTF station.

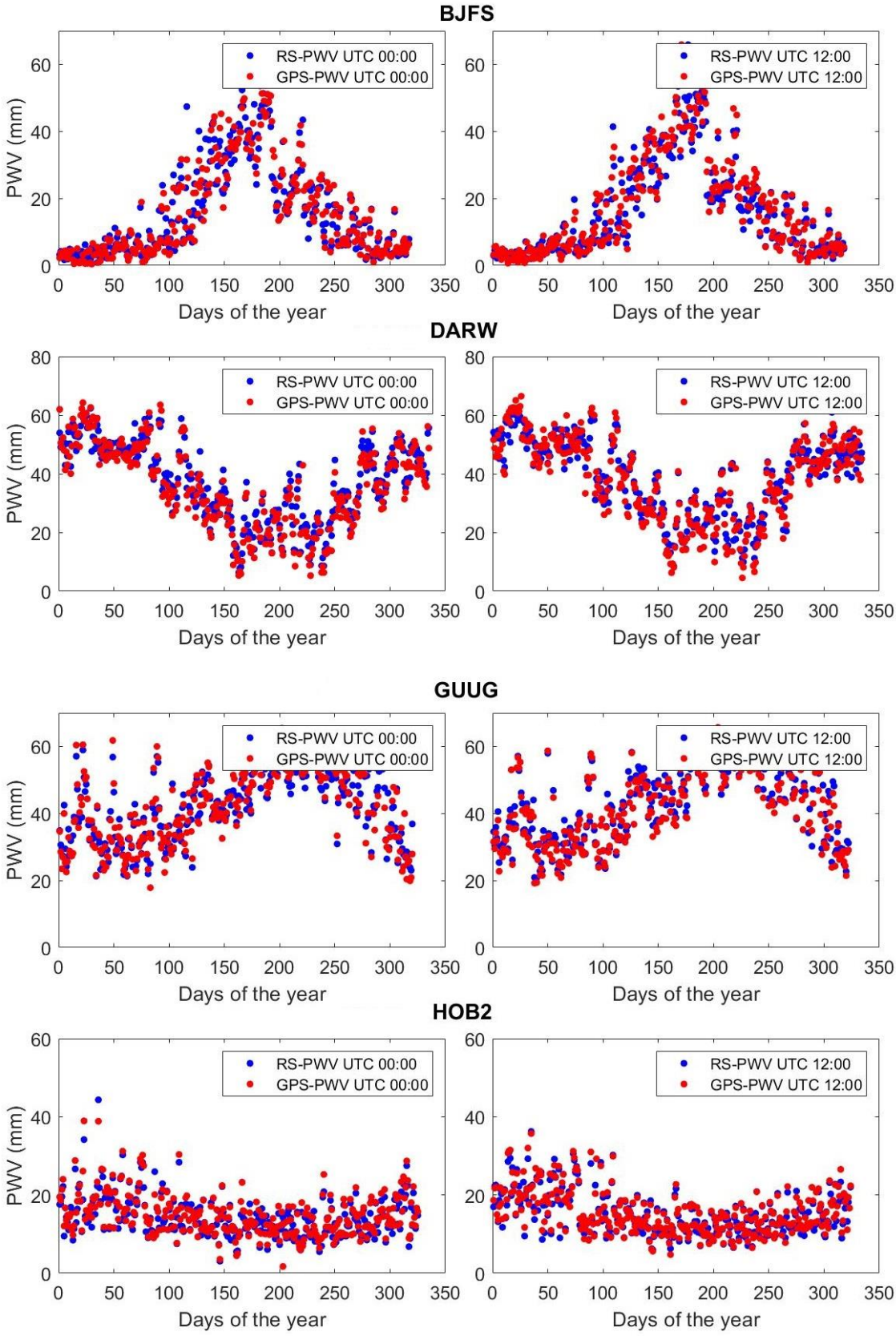

Fig. 9 Comparison of GPS-PWV estimates with the RS-PWV at 00:00 UTC and 12:00 UTC for BJFS, DARW, GUUG and HOB2 station. Left plot: PWV comparison at UTC 00:00. Right plot: PWV comparison at UTC 12:00.

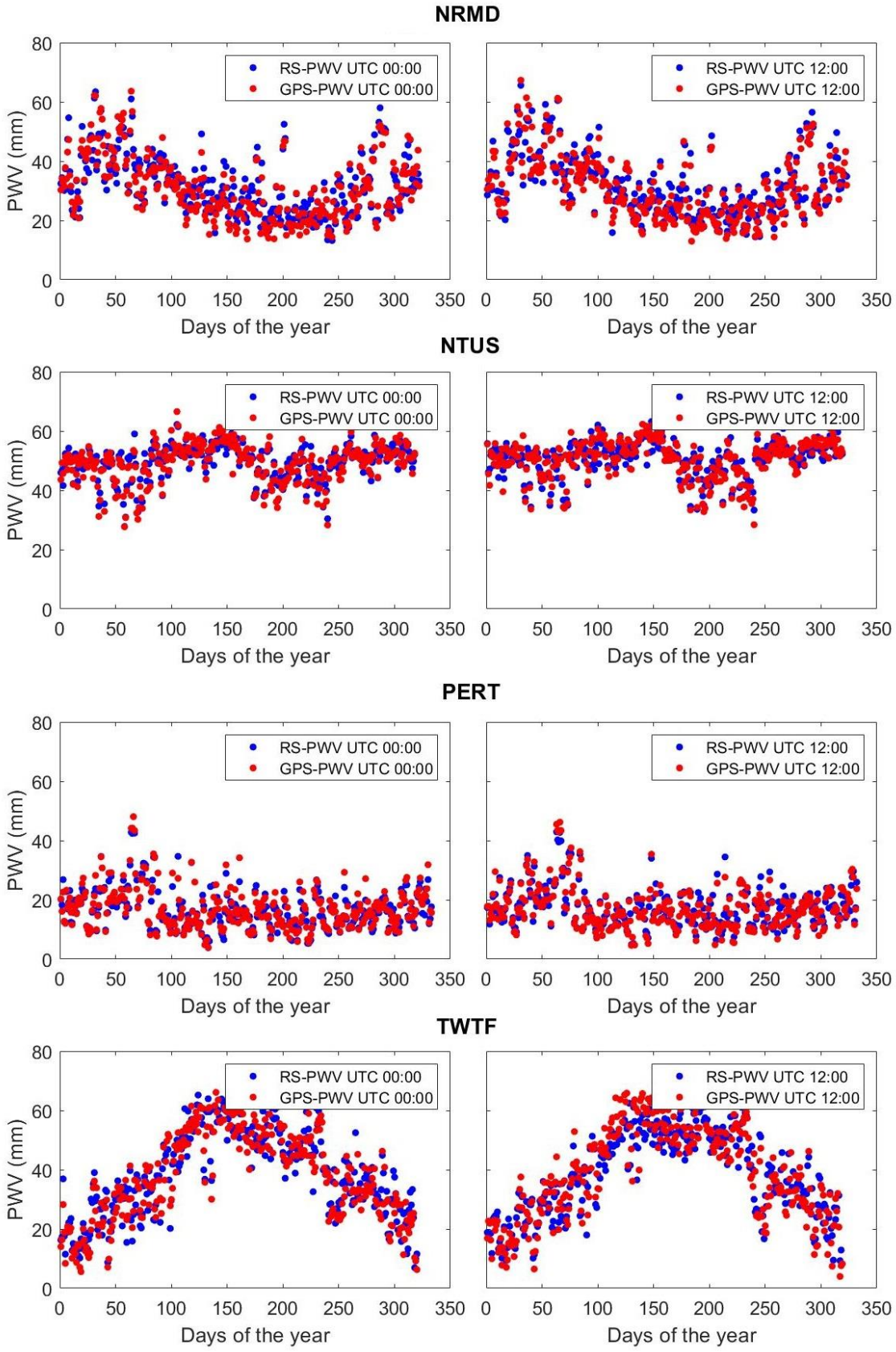

Fig. 10 Comparison of GPS-PWV estimates with the RS-PWV at 00:00 UTC and 12:00 UTC for NRMD, NTUS, PERT and TWTF station. Left plot: PWV comparison at UTC 00:00. Right plot: PWV comparison at UTC 12:00.

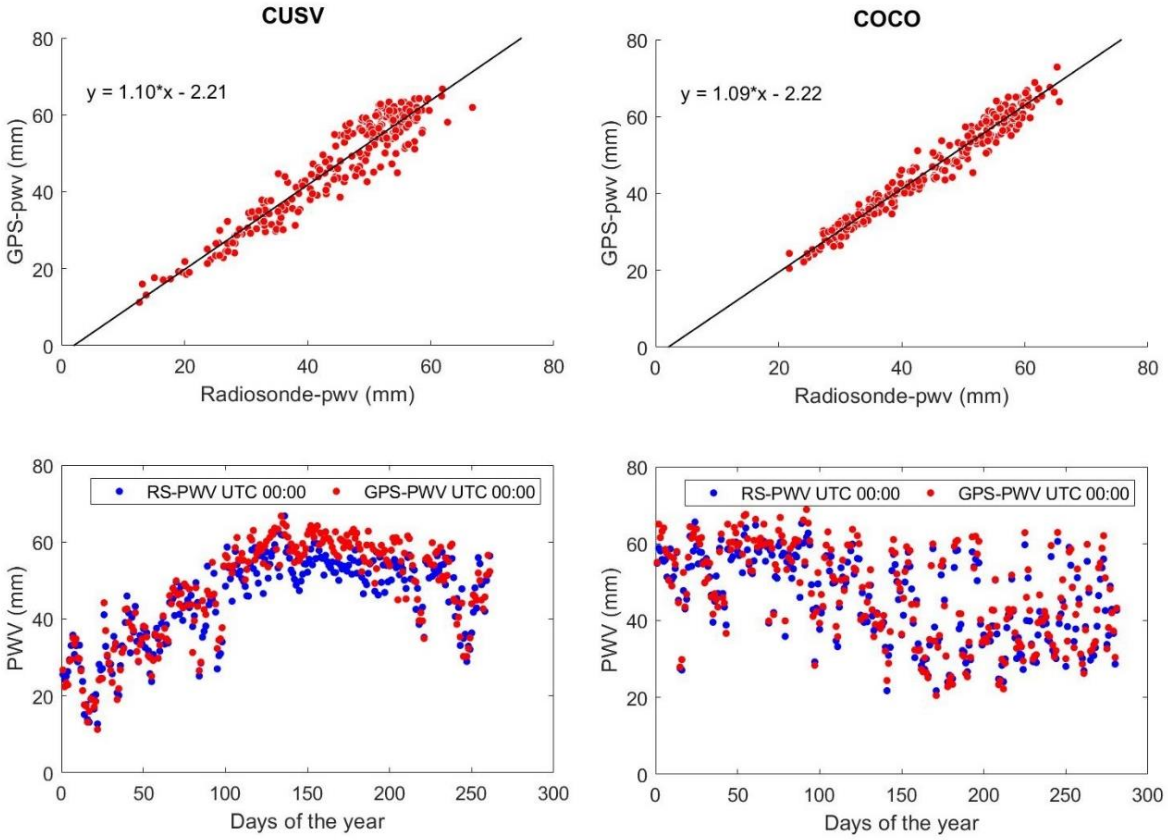

Fig. 11 Display of scatter plot and GPS PWV estimate against RS PWV measurements at UTC 00:00. Left plot: CUSV station Right plot: COCO station.

Table 12 Statistical summary of GPS-derived PWV and RS-measured PWV (00:00 UTC).

Site	UTC 00:00 R^2	Slope	Intercept	Bias	STD difference
BJFS	0.85	0.94	0.96	0.05	5.47
DARW	0.85	0.98	–0.08	–0.87	5.37
GUUG	0.95	1.11	–4.05	0.73	2.93
NTUS	0.86	1.05	-2.67	–0.40	2.40
HOB2	0.89	0.98	0.80	0.53	1.74
TWTF	0.82	0.93	2.21	–0.54	6.37
PERT	0.88	0.98	0.58	0.28	2.35
CUSV	0.9	1.10	–2.21	2.26	4.31
COCO	0.96	1.01	–2.20	1.69	2.59
NRMD	0.91	1.01	–1.36	–0.98	3.12
Mn	0.94	0.94	1.94	0.22	4.08

RS-measured PWV at 0000 UTC and 1200 UTC agreed well. Because outliers are present and therefore not disregarded in the statistical analysis, several stations show slightly larger standard deviation (STD) difference between GPS-PWV and RS-PWV. Results given in Tables 12 and 13 clearly demonstrate that mean bias between GPS-PWV and RS-PWV for BJFS and TWTF station at 12:00 UTC is larger than the bias value at 00:00 UTC. GPS-PWV values are underestimated than the RS-PWV. In addition, the bias for BJFS and TWTF station is 0.05 and 0.98 mm, and, -0.54 and 0.51 mm, at 0000 UTC and 1200 UTC, respectively. Additionally, minimum value of R^2 and STD difference between GPS-PWV and RS-PWV is 6.37 and 6.95 mm noticeable at TWTF site at 00:00 UTC and 12:00 UTC, respectively. On the other hand, mean bias for HOB2 and PERT station is 0.53 and 0.26 mm, 0.28 and -0.39 mm, at 00:00 UTC and 12:00 UTC, respectively. Moreover, bias for COCO which is coastal land site, mean bias reaches to 1.69 mm at 00:00 UTC. Moreover, average bias for DARW, NTUS and NRMD site at 00:00 UTC and 12:00 UTC reaches –0.87 to –1.59 mm, –0.40 to –0.22 mm and –0.98 to –1.47 mm, respectively. The

Table 13 Statistical summary of GPS-derived PWV and RS-measured PWV (12:00 UTC).

Site	UTC 12:00 R^2	Slope	Intercept	Bias	STD difference
BJFS	0.93	1.02	0.71	0.98	3.87
DARW	0.86	1	–1.74	–1.59	5.29
GUUG	0.97	1.04	–2.34	–0.74	2.11
NTUS	0.85	1.02	–1.37	–0.22	2.49
HOB2	0.96	0.98	0.47	0.26	1.08
TWTF	0.8	1	0.47	0.51	6.95
PERT	0.91	1.01	–0.56	–0.39	2.16
NRMD	0.94	0.99	–1.29	–1.47	2.68
Mn	0.95	0.96	1.63	–0.34	3.88

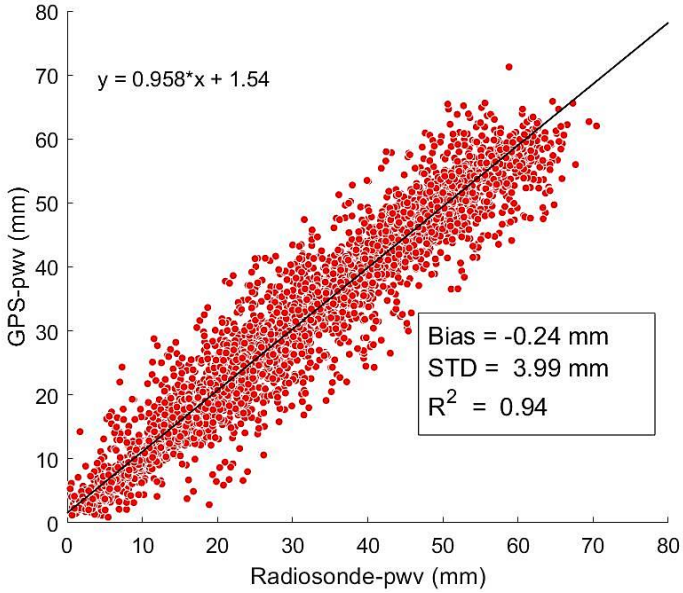

Fig. 12 Scatter plot of GPS PWV estimates against RS PWV measurements for eight site for both 00:00 UTC and 12:00 UTC.

negative bias showed that GPS-PWV values are higher than RS-PWV values. Moreover, it can be illustrated from results given in Table 12 and Table 13 that squared value of R is 0.85 to 0.96 at 00:00 UTC, and 0.80 to 0.96 at 12:00 UTC, respectively. Furthermore, mean bias and STD difference is 0.22 and 4.08 mm at 00:00 UTC, and –0.34 and 3.88 mm, respectively at 12:00 UTC. Figure 12 shows the scatter plot between the GPS derived PWV and RS PWV measurements for 8 stations. While Table 14 outlines the summary for the PWV comparison between GPS-PWV and RS-PWV for Figure 12. Over the duration of the study period, the average difference and STD between GPS-PWV and RS-PWV for the selected station is - 0.24 mm and 3.99 mm, respectively.

Figure 13 displays difference between GPS-PWV and RS-PWV values at 0000 UTC and 1200 UTC. By deducting the average PWV daily measurements for each station at 0000 UTC and 1200 UTC, PWV differences are calculated. The maximum and minimum difference between the RS-measured PWV and GPS-derived PWV is 9.33 to 18.61 mm and –8.0 to –16.54 mm, respectively. Moreover, the largest and smallest PWV difference value is noticeable for GUUG and TWTF station, respectively. The mean difference results vary significantly depending on the time of RS launch during daytime and nighttime period. In addition, the difference may be due to measurement error induced by radiosonde daylight solar heating (Ohtani and Naito, 2000; Kwon et al., 2007; Wang and Zhang, 2008). Furthermore, it could have been caused by a change in measurement time, or an area with complex topography. The sun's heat causes the humidity sensor to become drier during the day, which is the main reason of the increased dry bias for RS instruments.

4. SUMMARY AND CONCLUSION

The main purpose of this study is to investigate and validate the GPS data observations for analyzing ZTD and generating time series of PWV for use in

Table 14 Comparison results summary between the GPS-PWV and RS-PWV at eight sites.

Site	Max	Min	R^2	Bias	STD
BJFS	17.04	–14.79	0.89	0.52	4.76
DARW	17.22	–15.33	0.86	–1.23	5.34
GUUG	18.61	–14.75	0.95	0	2.65
NTUS	13.62	–7.84	0.86	–0.31	2.45
HOB2	12.55	–7.31	0.93	0.40	1.46
TWTF	15.13	–16.54	0.81	–0.01	6.69
PERT	9.33	–8.08	0.89	–0.05	2.28
NRMD	12.63	–10.74	0.92	–1.23	2.92

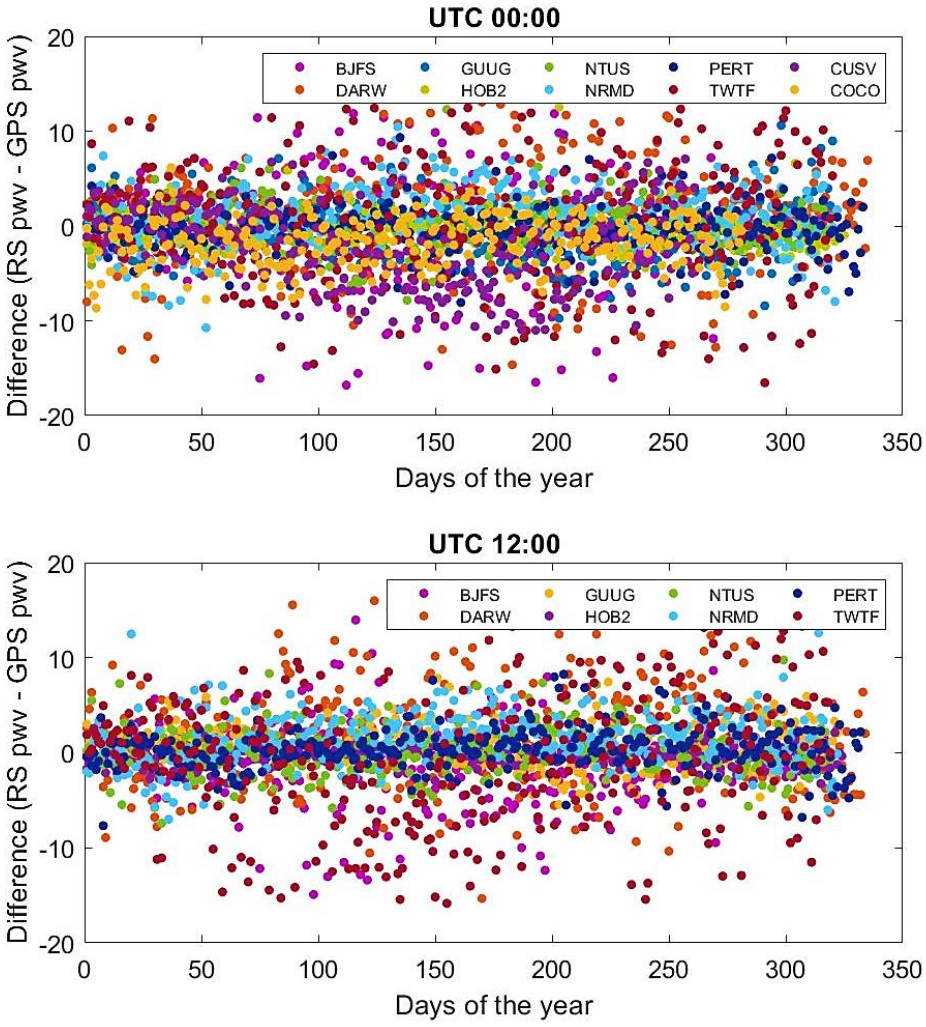

Fig. 13 Plot for difference between GPS-PWV estimates and RS-PWV measurements: (above) difference at UTC 00:00. (below) difference at 12:00 UTC.

climate studies and research in the Southeast Asian-Pacific area. One year of data observations from 20 permanent GPS stations is employed. At first stage of work, PPP ZTD estimates are obtained for each sites and average estimate of ZTD is 2.50 – 2.60 m during JF, AM, JA and ON time periods at stations latitude between 10°N – 10°S. This could be explained by the fact that the equatorial regions have distinct environmental conditions with varying meteorological factors (such as temperature and humidity). In addition, ZTD estimate for stations at higher mid-latitudes is 2.30 to 2.40 m. During the second part of study, GPS PWV estimate is determined, Results show that the average STD of GPS PWV estimate is 6.5, 7.9, 6.9 and 7.1 mm during JF, AM, JA and ON month study period, respectively. The average RMS and STD for GPS PWV estimate is 35.9 and 11.1 mm, respectively.

In the final stage of study, time series of GPS-PWV are assessed and compared with RS-PWV measurements from ten sites. The comparison of GPS-PWV with RS-PWV revealed an excellent agreement, with an average correlation of 0.96. Furthermore, the bias and STD between GPS PWV and RS measured PWV is -0.24 mm and 3.99 mm, respectively. Stations with bigger variability in PWV values include (1) those in the areas where atmospheric moisture is very high, and (2) those where there is a horizontal distance (< 60 km) between GPS and RS sites. In addition, the PWV in the subtropical coastal regions continued to be at a high level due to the influence of the water vapour from the Tropical Ocean. These findings are consistent with prior analyses and research work utilizing GPS data (Choy et al., 2015; Gui et al., 2017; Yeh et al., 2018; Ssenyunzi et al., 2020).

If GPS stations are collocated with surface weather and radiosondes launch sites, the accuracy of the PWV estimations can be increased. It has also been demonstrated that the accuracy of the PWV estimates is affected and varies with season, topography, and other local/regional climate factors. A viable and potential alternative to determine PWV is provided by GPS technology because of its high accuracy and temporal resolution. To mitigate the difference between the GPS-derived PWV and the radiosonde-PWV, more studies and research across data sets derived by various observation techniques may be significant and beneficial.

5. FUTURE WORK

The next stage of research study will look into the diurnal, semi diurnal and seasonal variations in PWV for minimum of four years of data observations.

ACKNOWLEDGMENTS

The authors acknowledge and thanks the IGS for providing GPS data and allowing us to download ZTD products. The authors also acknowledge NOAA for downloading the data used in this work.

REFERENCES

Abram, N.J., Wright, N.M., Ellis, B. et al.: 2020, Coupling of Indo-Pacific climate variability over the last millennium. Nature, 579, 385–392. DOI: 10.1038/s41586-020-2084-4

Alshawaf, F., Fuhrmann, T., Knöpfler, A. et al.: 2015, Accurate estimation of atmospheric water vapor using GNSS observations and surface meteorological data. IEEE Trans. Geosci. Remote Sens., 53, 7, 3764–3771. DOI: 10.1109/TGRS.2014.2382713

Bennitt, G.V. and Jupp, A.: 2012, Operational assimilation of GPS zenith total delay observations into the met office numerical weather prediction models. Mon. Weather Rev., 140, 8, 2706–2719. DOI: 10.1175/MWR-D-11-00156.1

Bevis, M., Businger, S., Herring, T.A. et al.: 1992, GPS meteorology: remote sensing of atmospheric water vapor using the global positioning system. J. Geophys. Res., 97, D14, 787–801. DOI: 10.1029/92jd01517

Boccolari, M., Fazlagić, S., Frontero, P. et al.: 2003, GPS Zenith Total Delays and precipitable water in comparison with special meteorological observations in Verona (Italy) during MAP-SOP. Ann. Geophys., 45, 5, 599–608. DOI: 10.4401/ag-3534

Boehm, J., Niell, A., Tregoning, P. and Schuh, H.: 2006a, Global Mapping Function (GMF): A new empirical mapping function based on numerical weather model data. Geophys. Res. Lett., 33, 3–6. DOI: 1029/2005GL025546

Boehm, J. and Schuh. H.: 2004, Vienna mapping functions in VLBI analyses. Geophys. Res. Lett., 31, 1, 2–5. DOI: 10.1029/2003GL018984

Boehm, J., Werl, B. and Schuh, H.: 2006b, Troposphere mapping functions for GPS and very long baseline interferometry from European Centre for Medium-Range Weather Forecasts operational analysis data. J. Geophys. Res., Solid Earth, 111. DOI: 10.1029/2005JB003629

Cao, Y., Guo, H., Liao, R. and Uradzinski, M.: 2016, Analysis of water vapor characteristics of regional rainfall around Poyang Lake using ground-based GPS observations. Acta Geod. Geophys., 51, 3, 467–479. DOI: 10.1007/s40328-015-0137-1

Choy, S., Wang, C.S., Yeh, T.K. et al.: 2015, Precipitable water vapor estimates in the Australian region from ground-based GPS observations. Adv. Meteorol., 5, 1, 1–14. DOI: 10.1155/2015/956481

Gleason, S and Gebre-Egziabher, D.: 2009, GNSS applications and methods. Artech House, 508 pp.

Gui, K., Che, H., Chen, Q. et al.: 2017, Evaluation of radiosonde, MODIS-NIR-Clear, and AERONET precipitable water vapor using IGS ground-based GPS measurements over China. Atmos. Res., 197, 461–473. DOI: 10.1016/j.atmosres.2017.07.021

Haffke, C. and Magnusdottir, G.: 2013, The South Pacific Convergence Zone in three decades of satellite images. J. Geophys. Res., 118, 839–849. DOI: 10.1002/jgrd.50838

Hakman, C., Guerova, G., Byram, S. et al.: 2015, International GNSS Service (IGS) troposphere products and Working Group activities. From the Wisdom of the Ages to the Challenges of the Modern World. Proc. the FIG Working Week 2015.

Hersbach, H., Bell, B., Berrisford, P., et al (2020) The ERA5 global reanalysis. Q. J. R. Meteorol. Soc., 146, 1999–2049. DOI: 10.1002/qj.3803

Jin, S.: 2012, Global navigation satellite systems – Signal, theory and applications. INTECH, 440 pp.

Jin, S., Cardellach, E. and Xie, F.: 2014, GNSS remote sensing: Theory, methods and applications. Springer, Dordrecht Heidelberg, 286 pp.

Jin, S. and Luo, O.F.: 2009, Variability and climatology of PWV from global 13-year GPS observations. IEEE Trans. Geosci. Remote Sens., 47, 7, 1918–1924. DOI: 10.1109/TGRS.2008.2010401

Kouba, J.: 2009, A guide to using International GNSS Service (IGS) products. Geod. Surv. Div. Nat. Resour., Canada, Ottawa, 6, 34.

Kuleshov, Y., Mcgree, S., Jones, D. et al.: 2014, Extreme weather and climate events and their impacts on island countries in the Western Pacific: Cyclones, floods and droughts. Atmos. Clim. Sci., 4, , 5, 803–818. DOI: 10.4236/acs.2014.45071

Kwon, H.T., Iwabuchi, T. and Lim, G.H.: 2007, Comparison of precipitable water derived from ground-based GPS measurements with radiosonde observations over the

Korean Peninsula. J. Meteorol. Soc. Japan, 85, 6, 733–746. DOI: 10.2151/jmsj.85.733

Malik, J.S., Jingrui, Z. and Khan, Z.Y.: 2020, Analysis of position coordinate accuracy of triple GNSS system by post-processing dual frequency observations using open source gamps: A case study. Acta Geodyn. Geomater., 17, 4, 485–499. DOI: 10.13168/AGG.2020.0035

Musa, T.A., Amir, S., Othman, R. et al.: 2011, GPS meteorology in a low-latitude region: Remote sensing of atmospheric water vapor over the Malaysian Peninsula. J. Atmos. Solar-Terrestrial Phys., 73, 16, 2410–2422. DOI: 10.1016/j.jastp.2011.08.014

Musa, T.A., Mazlan, M.H., Opaluwa, Y.D. et al.: 2017, Water vapour weighted mean temperature model for GPS-derived integrated water vapour in peninsular Malaysia. Int. Arch. Photogramm . Remote Sens. Spatial Inf. Sci., XLII/W5, 127–135. DOI: 10.5194/isprs-archives-XLII-4-W5-127-2017

Ohtani, R. and Naito, I.: 2000, Comparisons of GPS-derived precipitable water vapors with radiosonde observations in Japan. J. Geophys. Res. Atmos., 105, D22, 26917–26929. DOI: 10.1029/2000JD900362

Prange, L., Villiger, A., Sidorov, D. et al.: 2020, Overview of CODE's MGEX solution with the focus on Galileo. Adv. Sp. Res., 66, 12, 2786–2798. DOI: 10.1016/j.asr.2020.04.038

Saastamoinen, J.: 1972 Contributions to the theory of atmospheric refraction. Bull. Geodesique, 105, 279–298. DOI: 10.1007/BF02521844

Singh, D., Ghosh, J.K. and Kashyap, D.: 2014, Precipitable water vapor estimation in India from GPS-derived zenith delays using radiosonde data. Meteorol. Atmos. Phys., 123, 3-4, 209–220. DOI: 10.1007/s00703-013-0293-1

Ssenyunzi, R.C., Oruru, B., D'ujanga, F.M. et al.: 2020, Performance of ERA5 data in retrieving Precipitable Water Vapour over East African tropical region. Adv. Sp. Res., 65, 8, 1877–1893. DOI: 10.1016/j.asr.2020.02.003

Sun, Z., Zhang, B. and Yao, Y.: 2019, An ERA5-based model for estimating tropospheric delay and weighted mean temperature over China with improved spatiotemporal resolutions. Earth Sp. Sci., 6, 10, 1926–1941. DOI: 10.1029/2019EA000701

Trenberth, K.E.: 1997, The definition of El Nino. Bull. Am. Meteorol. Soc., 78, 12, 2771–2778. DOI: 10.1175/1520-0477(1997)078

Wang, J. and Zhang, L.: 2009, Climate applications of a global, 2-hourly atmospheric precipitable water dataset derived from IGS tropospheric products. J. Geod., 83, 3, 209–217. DOI: 10.1007/s00190-008-0238-5

Wang, J. and Zhang, L.: 2008, Systematic errors in global radiosonde precipitable water data from comparisons with groud-based GPS measurements. J. Clim., 21, 10, 2218–2238. DOI: 10.1175/2007JCLI1944.1

Yao, Y., Zhu, S., and Yue, S.: 2012, A globally applicable, season-specific model for estimating the weighted mean temperature of the atmosphere. J. Geod., 86, 5, 1125–1135. DOI: 10.1007/s00190-012-0568-1

Yao, Y., Zhang, B., Xu, C. and Yan, F.: 2014, Improved one/multi-parameter models that consider seasonal and geographic variations for estimating weighted mean temperature in ground-based GPS meteorology. J. Geod., 88, 3, 273–282. DOI: 10.1007/s00190-013-0684-6

Yeh, T.K., Shih, H.C., Wang, C.S. et al.: 2018 Determining the precipitable water vapor thresholds under different rainfall strengths in Taiwan. Adv. Sp. Res., 61, 3, 941–950. DOI: 10.1016/j.asr.2017.11.002

Zhang, Y., Wallace, J.M. and Battisti, D.S.: 1997, ENSO-like interdecadal variability : 1900 – 93. J. Clim., 10, 5, 1004–1020. DOI: 10.1175/1520-0442(1997)010

Zhang, Q., Ye, J., Zhang, S. and Han, F.: 2018, Precipitable water vapor retrieval and analysis by multiple data sources: Ground-based GNSS, radio occultation, radiosonde, microwave satellite, and NWP reanalysis data. J. Sensors, 1–13. DOI: 10.1155/2018/3428303

Zhao, Q., Yang, P., Yao, W. and Yao, Y.: 2020, Hourly PWV dataset derived from GNSS observations in China. Sensors, 20, 1, 231. DOI: 10.3390/s20010231

Zhou, F., Dong, D., Li, W. et al.: 2018, GAMP: An open-source software of multi-GNSS precise point positioning using undifferenced and uncombined observations. GPS Solut., 22, 2, 1–10. DOI: 10.1007/s10291-018-0699-9

Zumberge, J.F., Heftin, M.B., Jefferson, D.C. and Watkins, M.M.: 1997, Precise point positioning for the efficient and robust analysis of GPS data from large networks. J. Geophys. Res., 102, B3, 5005–5017. DOI: 10.1029/96JB03860